ELSEVIER

Journal of Crystal Growth 151 (1995) 180–186

JOURNAL OF CRYSTAL GROWTH

Preparation of Fe–Si single crystals and bicrystals for diffusion experiments by the electron-beam floating zone technique

V.N. Semenov [a], B.B. Straumal [a,b,*], V.G. Glebovsky [a], W. Gust [b]

[a] *Institute of Solid State Physics, Chernogolovka, Moscow District 142432, Russian Federation*
[b] *Institut für Metallkunde and Max-Planck-Institut für Metallforschung, Seestrasse 75, D-70174 Stuttgart, Germany*

Received 15 September 1994; manuscript received in final form 30 December 1994

Abstract

An electron-beam floating zone melting technique has been used to grow oriented single crystals and bicrystals of Fe–Si alloys with 6, 10, 12 and 14 at% Si. Procedures for the preparation of monocrystalline and bicrystalline seeds as well as for the growing of single crystals and bicrystals of these alloys are described. Studies of chemical composition of the bicrystalline specimens with aid of electron probe microanalysis revealed a homogeneous distribution of the main components. The behaviour of Fe–Si bicrystals in contact with a Zn-rich melt has been investigated. The wetting of grain boundaries by the melt and different types of Zn diffusion along the grain boundaries in several concentration intervals with a sharp transition from high to low diffusivity have been observed.

1. Introduction

Recent progress in the understanding of the structure and properties of grain boundaries (GBs) in pure metals was possible due to studies of bicrystals with well characterized individual GBs [1–3]. This progress was evoked by the development of the crystal growth techniques. A completely new and very promising field of investigation concerns the GB properties near the bulk phase transformations where the GBs have an unusual behaviour, especially in the case of second-order transformations. Fe–Si alloys are most promising for this purpose because they have a number of different bulk transformations of second order [4]. It is a challenge to the crystal growth techniques because crystallographically perfect bicrystals with individual GBs must be produced from alloys with a rather high solute concentration. Bicrystals of Fe–Si alloys with macroscopically flat and well defined GBs seem to be a good object for experimental studies of interesting GB phenomena such as diffusion along and across GBs, GB segregation and wetting of GBs by elements with a low melting point [5,6]. The chemical uniformity of bicrystals grown from highly pure alloys is of great interest for such experiments.

Three techniques, namely diffusion bonding, strain annealing and high-frequency floating zone melting are used to prepare bicrystals of Fe–Si alloys [7–9]. The bicrystals of Fe and dilute Fe–Si alloys were prepared by Lejcek et al. using diffusion bonding of two monocrystalline parts [7]. The authors concluded that the synthetic GBs are

* Corresponding author.

SSDI 0022-0248(95)00034-8

very clean and exhibit the same corrosion properties as natural GBs. The lattice parameter of single crystals of pure Fe and three Fe–Si alloys were measured on specimens grown by the strain-annealing method [8]. Kadechkova et al. [9] studied Fe–6at%Si bicrystals by Berg-Barret X-ray topography and showed that the stability of the temperature during the growth of bicrystals from the melt by the *high-frequency floating zone technique* must be at least as high as during the growth of highly perfect single crystals. The *electron-beam floating zone melting* (EBFZM) process is successively used for the purification and growth of crystals of highly pure refractory metals and alloys [9–11]. A possibility to melt refractory metals without crucibles, and, therefore, to have no contamination from crucible materials is one of the major advantages of the floating crucibleless melting techniques and especially of the electron-beam floating zone (EBFZ) technique. Metallic specimens are mostly heated and melted in crucibleless techniques by an electron beam or a high-frequency electromagnetic field. Electron-beam heating can be done in vacuum only, however, high-frequency electromagnetic field heating can be done both in vacuum and gaseous atmosphere.

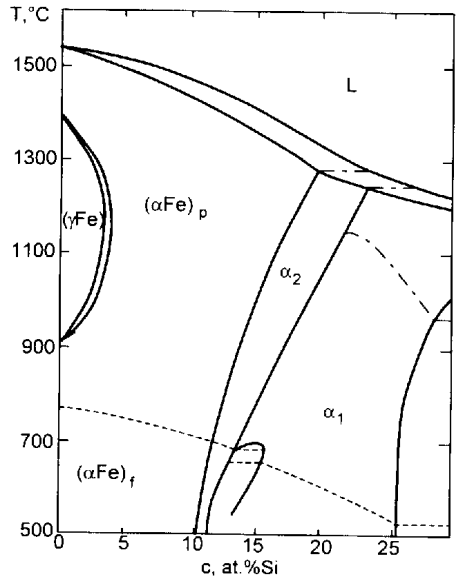

Fig. 1. A part of the Fe–Si phase diagram [4].

The vacuum EBFZM technique was used in the Institute of Solid State Physics, Chernogolovka, to prepare single crystals [11,12] and bicrystals [13] of high-purity refractory metals as well as to grow single crystals of Nb–Ta alloys [10] and Fe–Si alloys [14–16]. In this paper, we present results of experiments performed for growing Fe–Si alloys in a wide interval of Si concentrations (6, 10, 12 and 14 at% Si) together with the results of studies of different aspects of the behaviour of Fe–Si bicrystals. It has been shown that Fe–Si bicrystals of different crystallographic orientations can be grown by the vacuum EBFZM technique with a very homogeneous Si distribution along and perpendicular to the growth axis of the bicrystals.

2. Preparation of materials and growth of single crystals and bicrystals

For the further investigations of GB properties near the bulk phase transformations, Fe–Si alloys with 6, 10, 12 and 14 at%Si were chosen (Fig. 1) [4]. The concentration of Si in the alloy must be higher than 3.8 at% because for lower Si contents the α–γ transition does not permit to grow single crystals and bicrystals of these alloys. In Fe–6at%Si the ferromagnetic–paramagnetic transformation proceeds at about 740°C. In Fe–12at%Si the chemical A2–B2 ordering proceeds at about 760°C. The other two alloys (Fe–10at%Si and Fe–14at%Si) were chosen for comparison and in order to have a possibility to separate the influence of the bulk phase transformation on the GB properties. In these alloys no α–γ phase transformation proceeds. The Fe–10at%Si alloy remains paramagnetic and chemically disordered up to the melting point and the Fe–14at%Si alloy has an ordered B2 structure. These conditions define a rather narrow admissible concentration interval for each alloy (except Fe–6at%Si).

The alloys were prepared from 5N Si and 4N Fe. Commercial carbonyl iron was purified in vacuum by electron-beam melting. The concentration of impurities in the cast ingots of iron was analysed by spark-source mass spectrometery, atomic absorption, neutron activation and com-

bustion techniques. The total content of impurities was less than 10^{-2} wt%. The alloys were prepared using the *high-frequency levitation melting*. During this process the solid metal specimens were suspended in an electromagnetic field and melted by an induced electric current. The resulting liquid drops are spherical and slightly deformed by the interaction of the supporting electromagnetic field, the surface tension and the gravitation forces. To solidify liquid drops, it is enough to switch off the electric power. Then the melt is cast into cylindrical copper moulds and solidified to form rods of up to 25 g weight, 40 mm length and 10 mm diameter. Specimens of Fe–Si alloys were levitated in a vacuum chamber by special coils using a 440 kHz electric generator. This technique needs no crucibles and provides a homogeneous mixing of the elements in the liquid state. Further these ingots were remelted with aid of the high-frequency melting process in a refractory crucible using a high-vacuum furnace of 100 kW power. The main difference of this furnace from the standard ones is the possibility to cast a melt of 5 kg into a specially designed copper mould and to prepare a series of cylindrical ingots of 200 mm length and 18 mm diameter.

Single crystals of Fe–Si alloys were grown in a vacuum electron-beam floating zone melting apparatus [17]. To stabilize the temperature distribution in the liquid zone, a circular water-cooled copper electron gun was used (Fig. 2). The circular electron beam was emitted by a cathode of 60 mm diameter, made of 1 mm thick tungsten wire, and focused on the specimen with the aid of several electrodes. The specimen to be melted was the anode, set coaxially with the electron gun. An electric power supply produced an accelerating voltage of 5–25 kV and an anode current of 0.1–1 A. The electron gun could be moved vertically along the growth axis of the specimen with a rate of 0.5–50 mm/min. To prepare *monocrystalline seeds* of different orientations, a crystallographically perfect single crystal was grown and cut to obtain cylindrical pieces of 15–20 mm length and 10–25 mm diameter. Two parallel surfaces of a seed were checked carefully by X-ray diffraction with an accuracy of about 1°

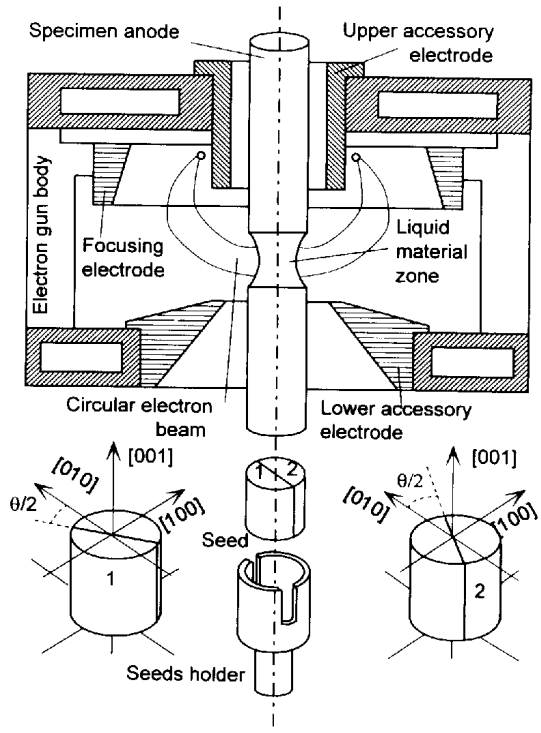

Fig. 2. The principal scheme of an electron gun and the geometry of the bicrystal growth with aid of the electron beam floating zone (EBFZ) technique. The scheme for cutting seeds for a ⟨001⟩{001} tilt GB with the misorientation angle θ is also shown.

and then polished in order to make very clean and mirror-like surfaces. Before growing, the lower holder with a seed on top of it, a cylindrical ingot and an upper holder are joined together by in-situ local electron-beam welding of the contacting surfaces. The *seeding procedure* consists of melting of a narrow liquid zone in the seed just under the seed/ingot interface. After an initial liquid zone is created, the electron gun is being moved up vertically together with the liquid zone until the whole specimen would become single crystalline.

In principle, the *growing procedure for Fe–Si bicrystals* is similar to that for single crystals. The bicrystalline seeds need a similar careful preparation as monocrystalline ones but because they are made up of two half-cylinders, the quality of the interface between them is of great importance. They had to be carefully ground, etched and polished to obtain clean and flat surfaces to be

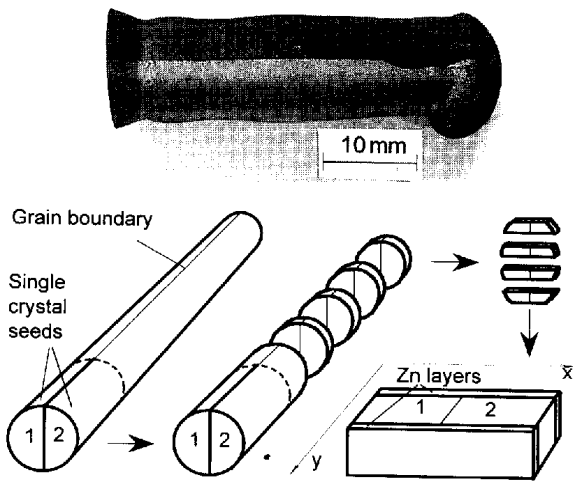

Fig. 3. The photograph of an Fe–10at%Si bicrystal grown with aid of the EBFZ technique together with the scheme of the sample cutting for the further experiments.

joined together. The bicrystalline seeds are composed using two single-crystalline halves (Fig. 1). The misorientation angle θ of a tilt GB is formed by oriented cutting of single crystals. Fig. 3 shows the photograph of a Fe–10at%Si bicrystal together with the scheme for sample cutting and preparation of specimens used for the GB investigations. Firstly, the seeds are removed by spark erosion. Only the 30–40 mm long part of the bicrystals close to the seeds is used for the further investigations. This part of the bicrystals is then cut perpendicular to the growth axis in about 2 mm thick slices. The elongated samples are then cut from these slices in such a way that the GB is in the middle of the long dimension of each sample and perpendicular to it (see Fig. 3). These samples are carefully polished on a 4000 grit SiN paper and chemically polished in a 80 ml H_2O_2–14 ml H_2O–6 ml HF solution. A 100–200 μm thick Zn layer is applied on the surface of each sample by immersing the specimen in a melt of 5N Zn at about 500°C. Then the Zn layer is partially removed from the two opposite sides of the bicrystal. Therefore, only two (001) surfaces of the bicrystal remained coated with Zn. The Zn coated samples are encapsulated in evacuated ($< 5 \times 10^{-4}$ Pa) silica tubes together with a piece of Ta foil as an oxygen getter and annealed at different temperatures maintained within ± 2°C in a tube furnace. The annealed samples are mounted in Wood's alloy and ground and polished with a 1 μm diamond paste. Electron probe microanalysis (EPMA) measurements are carried out by wave length dispersive analysis on a JEOL 6400 electron probe microanalyser operated at 15 kV. The intensities of the Fe Kα, Si Kα and Zn Kα peaks are determined, and from them the Fe, Si and Zn concentrations are obtained using a standard program for quantitative EPMA analysis.

3. Results

Fig. 4 presents the Si profiles measured by EPMA on the cross-sections of four Fe–Si bicrystals perpendicular to the growth axis. For a bicrystal with a nominal Si content of 12 at%, two curves are shown which are measured on two slices: cut at the beginning and at the end of the 30 mm long part of the bicrystal chosen for the further experiments. In our previous studies it was observed that the contact angle between the Zn-rich melt and GB in Fe–Si alloys can be very low and the liquid phase can penetrate rather deep along the GB into the bicrystal [14–16]. Besides, the observed GB diffusivity of Zn is very

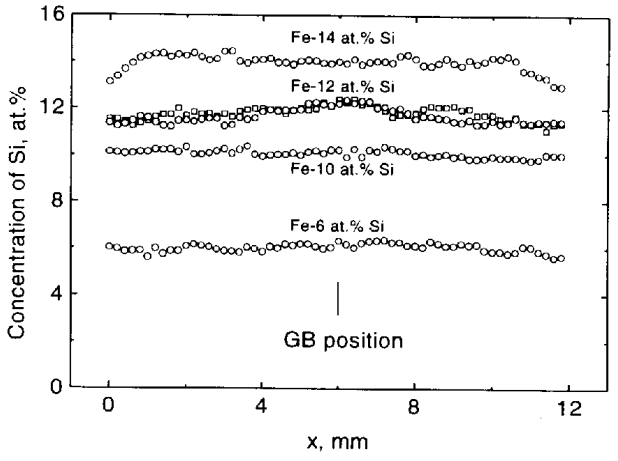

Fig. 4. Si distribution perpendicular to the growth direction and GB plane in four Fe–Si bicrystals with different Si contents. For Fe–12at%Si, the profiles are shown for two different cross-sections along the growth axis (the distance between the sections is about 30 mm).

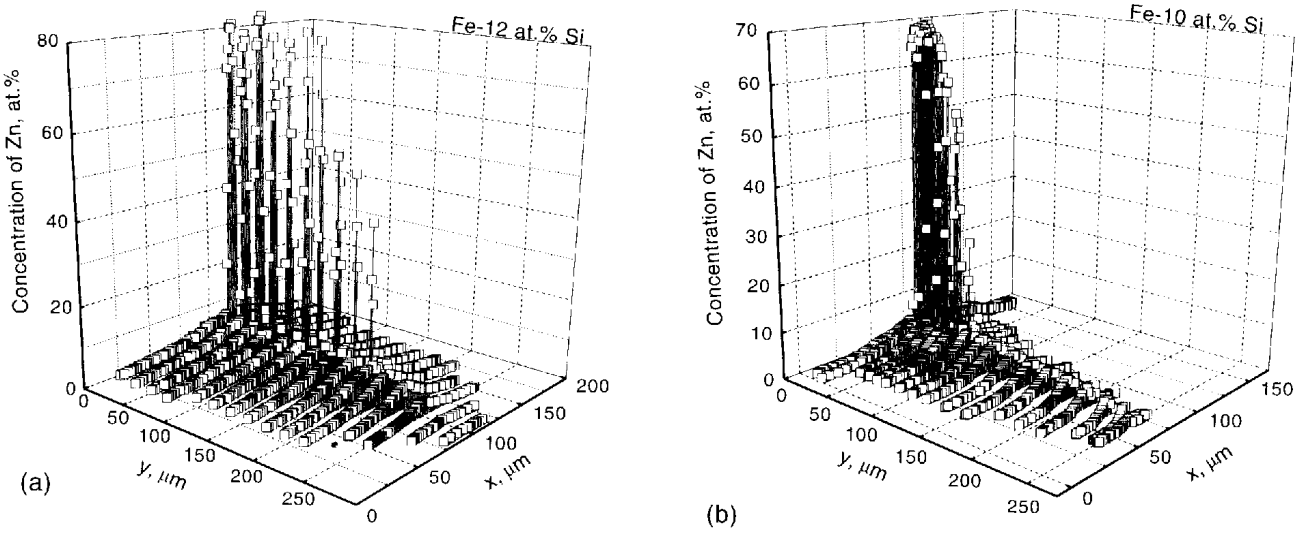

Fig. 5. Zn distribution in Fe–12at%Si (a) and Fe–10at%Si (b) bicrystals with a symmetrical 38.5°⟨001⟩{001} tilt GB after annealing at 994°C for 1.5 h and 720°C for 36.25 h, respectively.

different for different concentration intervals of Zn and Si. In some cases, the parameters of GB Zn diffusion are comparable with the data for GB tracer diffusion and self-diffusion in Fe–Zn and Fe–Zn–X alloys. In other cases, at Zn concentrations c close to the solubility limit of Zn in the corresponding Fe–Si alloy (c_0), the GB diffusivity of Zn is unusually high with a sharp change to the "normal" value at a concentration c_t ($c_t < c_0$). These two situations were carefully studied with the aid of EPMA. In Figs. 5 and 6 the concentration profiles are presented for bulk and GB diffusion of Zn in Fe–12at%Si and Fe–10at%Si bicrystals with a symmetrical 38.5°⟨001⟩{001} tilt GB after annealing at 994°C for 1.5 h and 720°C for 36.25 h, respectively.

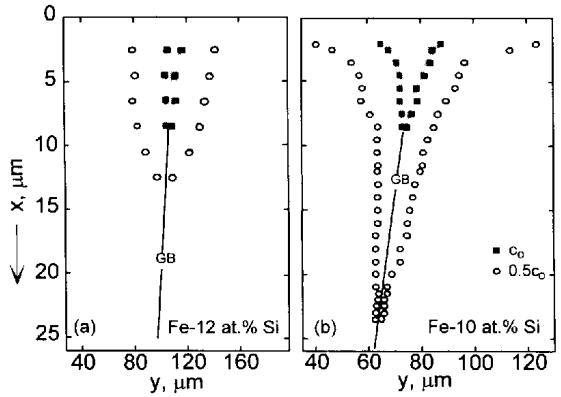

Fig. 6. Isoconcentrational $x-y$ sections of the Zn distributions shown in Fig. 5 for Zn concentrations c_0 and $0.5c_0$. In the shaded area is $c > c_0$.

In the three-dimensional plots of Fig. 5, the Zn distribution is shown on sections pependicular to the {100} surface of bicrystals coated with Zn (for the geometry of the sample see Figs. 2 and 3). Fig. 6 shows the isoconcentrational x–y sections for two different Zn concentrations, namely for the solubility limit c_0 of Zn in solid solution and for about $0.5c_0$. The concentration c_0 marks the interface between the solid solution and the Zn-rich melt. In the shaded area is $c > c_0$, and there is a melt at the annealing temperature.

4. Discussion

The Si profiles shown in Fig. 4 reveal good uniformity of the Si distribution in a cross-section perpendicular to the growth axis. Only at higher Si contents, the concentration of Si near the growth axis is about 0.5 at% higher than in the peripheral area. This difference can originate from the solidification process. Therefore, for further experiments only the central parts of such bicrystals are used. The two Si profiles for the

bicrystal with a nominal Si content of 12 at% are measured on two slices prepared from the beginning and end of the 30 mm long part of the bicrystal which was chosen for the further experiments. Both curves coincide rather well. They do not reveal distinct differences in the cross-sectional Si distribution along the growth axis. The average concentrations of Zn also coincide rather well with the nominal concentrations of 6, 10, 12 and 14 at% Si. It means that the technique guarantees the production of bicrystals with a chemical composition of alloys very close to the nominal one.

The Zn distribution shown in Figs. 5a and 5b indicates an important feature of the interaction of a GB in Fe–Si alloys with a Zn-rich melt. The Zn-rich melt penetrates deep into the bicrystal along the GB resulting in Zn concentrations up to 60–80 at%. Our experiments show that the length of this molten area depends primarily on the thickness of the Zn layer deposited on the specimen surface before annealing and does not depend on the anneal duration. Therefore, the formation of this layer is the result of a partial dissolution of the Fe–Si alloy in the molten Zn during the heating of bicrystals at the beginning of a diffusional anneal according to the Fe–Si–Zn phase diagram [18]. If the Zn layer is thick enough, the molten phase penetrates along the GB and separates the bicrystal into two single crystalline parts (Fig. 7c). This means that the GB energy (σ_{GB}) is lower than $2\sigma_{SL}$ (σ_{SL} being the energy of the solid/liquid interface) and the liquid phase wets the GB completely. In this case the contact angle, θ, between the GB and both solid/liquid interfaces is equal to zero.

The Zn-rich layer, which replaced a part of the GB, acts as a source for the GB and bulk diffusion during annealing. It follows the primary dissolution stage. The uniform layer of bulk diffusion can be seen on the left and right sides of the wetted GB part (Figs. 5 and 6). The situation for GB diffusion is very different for the two samples investigated. In the Fe–12at%Si sample, the diffusion layer along the GB is not deeper than the layer of the bulk diffusion (Figs. 5 and 6). For the Fe–10at%Si sample, the situation is completely different (Figs. 5 and 6). Below the layer of the Zn-rich phase there is an area about 150 μm long where Zn diffuses along the GB very fast. At the concentration c_{bt} there is a break in the GB penetration curve of Zn. Below this concentration, the Zn diffusivity is low and the GB penetration curve is very similar to the bulk one. In Refs. [14–16] a model was proposed that between c_0 and c_{bt} a layer of a quasi-liquid GB phase exists with a high diffusivity. The layer of this phase, which is not stable in the bulk, can be stable under some conditions at the GB. The sudden change of the diffusivity at the concentration c_{bt} is driven by the formation of this GB layer of a liquid-like phase, the so-called premelting GB phase transition. This hypothesis was supported by the numerous experiments made using Fe–Si bicrystals grown by us.

5. Conclusions

The electron-beam floating zone melting technique was developed for growing oriented single crystals and bicrystals of Fe–Si alloys with a rather high concentration of Si. Bicrystals with ⟨001⟩{001} tilt GBs of Fe–6at%Si, Fe–10at%Si, Fe–12at%Si and Fe–14at%Si were successfully grown. In Fe–6at%Si and Fe–12at%Si the bulk phase transitions of second order proceeded, correspondingly ferromagnetic–paramagnetic and A2–B2 chemical ordering transitions. In this case the well characterized GB will not be destroyed by the phase transformations, it will exist both above and below the temperatures of these transformations. The high uniformity of the Si concentration along and across the growth axis of the bicrystals allowed experiments to be performed to study the influence of bulk phase transformations on the GB wetting and GB diffusion of Zn. For the first time, these experiments revealed indirectly the existence of the so-called GB premelting phase transitions.

Acknowledgements

The authors wish to thank Prof. L.S. Shvindlerman, Dr. E. Bischoff and Mr. V. Lomeiko for

fruitful discussions and helpful assistance. This work was partly supported by the Volkswagen Foundation and the International Science Foundation (under contract RER000).

References

[1] B.B. Straumal and L.S. Shvindlerman, Acta Met. 33 (1985) 1735.
[2] T. Muschik, W. Gust, S. Hofmann and B. Predel, Acta Met. 37 (189) 2917.
[3] R. Schmelzle, B. Giakupian, T. Muschik, W. Gust and R.A. Fournelle, Acta Met. Mater. 40 (1992) 997.
[4] T.B. Massalski et al., Eds., Binary Alloy Phase Diagrams (ASM International, Metals Park, Ohio, 1990) p. 1772.
[5] E.I. Rabkin, L.S. Shvindlerman and B.B. Straumal, Intern. J. Mod. Phys. B 5 (1991) 2989.
[6] C.S. Pande and Y.T. Chou, in: Treatise on Materials Science and Technology, Vol. 8, Ed. H. Herman (Wiley, London, 1975) p.43.
[7] P. Lejcek, E.A. Stepankov and S. Kadeckova, Proc. 6th Intern. Symp. on High-Purity Materials, Dresden (1985) p. 21.
[8] M. Polkarova, K. Godwod, J. Bak-Misiuk, S. Kadeckova and J. Bradler, Phys. Status Solidi (a) 106 (1988) 17.
[9] S. Kadeckova, P. Toula and J. Adamek, J. Crystal Growth 83 (1987) 410.
[10] V.G. Glebovsky and B.M. Shipilevsky, J. Crystal Growth 60 (1982) 363.
[11] V.G. Glebovsky, V.N. Semenov and V.V. Lomeyko, J. Crystal Growth 87 (1988) 142.
[12] V.G. Glebovsky, V.N. Semenov and V.V. Lomeyko, J. Vacuum 41 (1990) 2165.
[13] V.G. Sursaeva, V.G. Glebovsky, Yu.M. Shulga and L.S. Shvindlerman, Scripta Metall. 19 (1985) 411.
[14] E.I. Rabkin, V.N. Semenov, L.S. Shvindlerman and B.B. Straumal, Acta Met. Mater. 39 (1991) 627.
[15] O.I. Noskovich, E.I. Rabkin, V.N. Semenov, B.B. Straumal and L.S. Shvindlerman, Acta Met. Mater. 39 (1991) 3091.
[16] B.B. Straumal, O.I. Noskovich, V.N. Semenov, L.S. Shvindlerman, W. Gust and B. Predel, Acta Met. Mater. 40 (1992) 795.
[17] V.G. Glebovsky, V.V. Lomeyko and V.N. Semenov, J. Less-Common Metals 117 (1986) 385.
[18] W. Köster, Metallurgia 80 (1969) 219.